Mach Number Estimation and Pressure Profile Measurements of Expanding Dense Organic Vapors

Head, Adam J.; Michelis, Theodoros; Beltrame, Fabio; Fuentes-Monjas, Blanca; Casati, Emiliano; Servi, Carlo De; Colonna, Piero

DOI
10.1007/978-3-031-30936-6_23

Publication date
2023

Document Version
Final published version

Published in
ERCOFTAC Series

Citation (APA)
Head, A. J., Michelis, T., Beltrame, F., Fuentes-Monjas, B., Casati, E., Servi, C. D., & Colonna, P. (2023). Mach Number Estimation and Pressure Profile Measurements of Expanding Dense Organic Vapors. In M. White (Ed.), *ERCOFTAC Series* (pp. 229-238). (ERCOFTAC Series; Vol. 29). Springer. https://doi.org/10.1007/978-3-031-30936-6_23

Mach Number Estimation and Pressure Profile Measurements of Expanding Dense Organic Vapors

Adam J. Head[1(✉)], Theodoros Michelis[1], Fabio Beltrame[1], Blanca Fuentes-Monjas[1], Emiliano Casati[2], Carlo De Servi[1,3], and Piero Colonna[1]

[1] Propulsion and Power, Delft University of Technology, Delft, The Netherlands
{a.j.head,t.michelis,f.beltrame,
c.m.deServi,p.colonna}@tudelft.nl
[2] Department of Mechanical and Process Engineering, ETHZ, Zürich, Switzerland
casatie@ethz.ch
[3] Energy Technology Unit, VITO, Mol, Belgium
carlo.deservi@vito.be

Abstract. This paper describes an experiment conducted within the nozzle test section of the Organic Rankine Cycle Hybrid Integrated Device (ORCHID) aimed at providing accurate data for the validation of NICFD flow solvers [5]. A supersonic flow of the dense vapor siloxane MM established in the nozzle of the setup was characterized by means of the schlieren technique and by pressure taps along the nozzle profile. The nozzle inlet conditions corresponded to a stagnation temperature and pressure of $T_0 = 253$ °C and $P_0 = 18.36$ bara. At these inlet conditions, the compressibility factor of the fluid is $Z_0 = 0.58$. The nozzle backpressure was equal to $P_b = 2.2$ bara. The experimental data-set includes: 1) the average mid-plane local Mach number, which was derived from the schlieren images by estimating the angle of the Mach waves originating from the roughness of the upper and lower nozzle surfaces, 2) the angle of a shock wave generated by a 5° wedge placed at the nozzle exit, also detectable in the schlieren images, and 3) the static pressure distribution along the flow expansion acquired with a *Scanivalve* DSA3218 pressure scanner device. The Mach number at the nozzle exit estimated based on the schlieren images is $M = 1.95 \pm 0.05$, very close to the expected value of $M = 2$ according to the design conditions of the experiment. The static pressure measurements have a maximum absolute uncertainty amounting to ± 1.80 kPa in the initial stages of the expansion. This information was used to assess the capability of the open-source SU2 flow solver in evaluating the NICFD effects in a supersonic flow of MM when the fluid thermodynamic properties are modeled with a cubic equation of state. For this purpose, two-dimensional Euler simulations were carried out with SU2 for the operating conditions achieved in the experiment. The numerical results are in good agreement with the experimental data. The largest deviation between the simulation and experiment is observed in the nozzle uniform region, where two dips in the Mach number occur due to a slight local decrease in flow velocity owing to two weak shock waves. The shock wave generated by the wedge located at the nozzle

M. White et al. (Eds.): NICFD 2022, ERCOFTAC 29, pp. 229–238, 2023.
https://doi.org/10.1007/978-3-031-30936-6_23

outlet propagates with two different angles, namely, $\beta_{\text{above}} = 37.6^\circ \pm 0.86$, and $\beta_{\text{below}} = 31.6^\circ \pm 0.64$, due to the axial misalignment of the wedge with respect to the flow.

Keywords: Schlieren measurements · data processing · error identification and uncertainty estimation

1 Introduction

The computer simulation of compressible flows is critical to the development of advanced technologies, like airplanes and aero-engines, rockets, and gas turbines, to name a few. Over the past few decades, CFD codes have reached a remarkable level of accuracy because of the extensive availability of accurate experimental data for their verification and validation [11]. However, these experimental data sets are limited to aerodynamic flows or classical and ideal gas dynamics. There is limited data available for flows typically encountered in the research subject of Non-Ideal Compressible Fluid Dynamics (NICFD), such as transcritical expansions close to the critical point and compressible two-phase flows. Although first experimental results on non-ideal compressible effects in supersonic flows of dense organic vapours have been recently published, see Ref. [2, 12, 14], the data in the literature remain insufficient in terms of quantity and quality for the validation of NICFD-capable flow solvers.

The Organic Rankine Cycle Hybrid Integrated Device (ORCHID) of the Propulsion and Power laboratory of the Delft University of Technology was built for this reason [5]. Notably, the setup is currently equipped with a nozzle test section to generate paradigmatic supersonic flow test cases similarly to what is done for classical and ideal gas dynamics, but for flows in the NICFD regime. The objective is to accurately measure quantities in the flow established in a convergent divergent nozzle, either empty or with an obstacle inserted to generate shock waves, for the validation of CFD codes capable of simulating NICFD flows.

This paper reports the results of an experimental campaign executed inside the ORCHID nozzle test section. In particular, datasets have been generated for: i) the total conditions at the inlet and outlet of a planar nozzle; ii) thanks to schlieren imaging, Mach lines over the entire length of the diverging part of the nozzle, and a shock-wave generated by a 5° wedge positioned at the exit of the nozzle in the testing channel; and, iii) static pressure measurements along the upper and lower surfaces of the planar nozzle. To ensure the reproducibility of the experimental test cases with a CFD model, a method for tracking the nozzle geometry, which changes position due to thermal expansion of the nozzle housing, was developed. Furthermore, uncertainties associated to the measured quantities have been calculated and reported.

The paper is structured as follows. Section 2 presents the layout of the nozzle test section together with the pressure measurement instrumentation. Furthermore, the schlieren layout and measurement procedure together with the specifications of the experiment are defined. In Sect. 3 the schlieren data post processing method and the

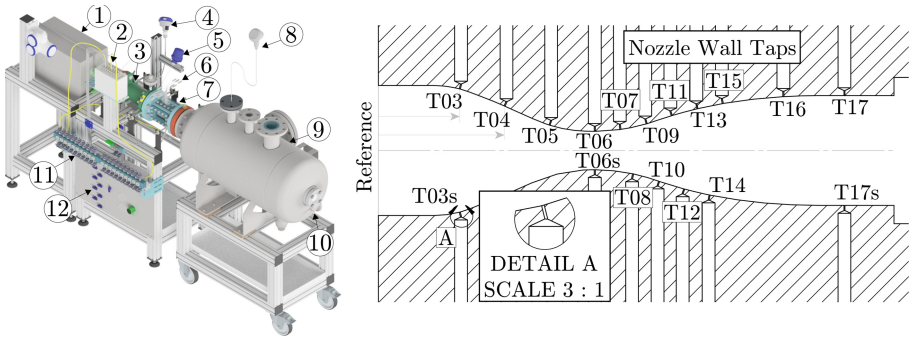

(a) (b)

Fig. 1. The primary components and instrumentation of the nozzle TS. **(a).** ①: Flow Meter *KROHNE OPTIMASS 6400 F F* – Tag FT0004; ②: *Scanivalve DSA3218*; ③: Settling Chamber; ④: *WIKA UPT 20* – Tag PT011; ⑤: *WIKA TR10-C PT100* – Tag TT015; ⑥: *Taps*; ⑦: Nozzle Housing; ⑧: *WIKA UPT 20* – Tag PT014; ⑨: Receiver; ⑩: *WIKA TR10-C PT100* – Tag TT014; ⑪: Liquid Trap; ⑫: Scanivalve Control Panel. **(b).** A cross-section of the planar nozzle showing the positioning of the eighteen pressure taps. Three taps are symmetrically aligned and are indicated by the letter s. Detail A shows that the opening of each tap is perpendicular to the nozzle profile wall. Distances to taps from Reference in [mm]: T03(s) = 15.96; T04 = 24.72; T05 = 33.55; T06(s) = 42.4; T07 = 47.44; T08 = 49.9; T09 = 52.57; T10 = 55.01; T11 = 57.5; T12 = 59.91; T13 = 62.53; T14 = 64.89; T15 = 67.47; T16 = 79.35; T17(s) = 91.3. Two taps, T01 & T02, are located in the settling chamber at the first and second flange. Nozzle profile designed for the MM working fluid at the design conditions: $T_0 = 252$ °C, $P_0 = 18.4$ bar and a back pressure of 2.1 bar with a throat height $H_{\text{th}} = 7.5$ mm. See Nozzle B in [5, App. B] for the geometric points defining the profile. Fluid properties estimated with the multi-parameter equation of state available in the thermophysical property database of NIST [8].

uncertainty estimation of the experiment error sources is presented. Section 4 reports the average midline Mach number distribution in the diverging part of the planar nozzle together with the associated uncertainties. Furthermore, the pressure field obtained with a pressure scanner is also shown. The experimental results are also compared with the predictions of a CFD model. The conclusions and an outlook for future work are presented in Sect. 5.

2 The Nozzle Test Section: Layout and Measurement Procedure

Fig. 1a shows an isometric view of the ORCHID nozzle test section (TS) including the system instrumentation. A complete detailed overview of the main TS components, namely, the settling chamber ③, nozzle housing ⑦ and the receiver ⑨ can be found in [5, Ch. 6]. Figure 1b shows the converging diverging nozzle profile which has been designed with the method of characteristics [4]. The nozzle is made from two equal and removable profiles, which are inserted at the top and bottom of the nozzle housing.

The side walls of the nozzle are made from transparent windows which provide optical access.

Two pressure transmitters *Wika UPT 20*, see ④ & ⑧, are used to characterise the total pressure in the settling chamber and the pressure in the receiver. Both pressure transmitters have an expanded uncertainty of ± 0.1 bar. The test section is also equipped with a *Scanivalve* (SV) DSA3218 pressure scanner ② which is used, in combination with pressure taps, to measure the static pressures along the nozzle profile. The DSA3218 is a stand-alone digital pressure scanner which can accept up to 16 pneumatic inputs (ports $P_{SV}001$ to $P_{SV}016$) where each input is connected to a discrete pressure transducer. In particular, it incorporates 16 temperature compensated piezoresistive pressure transducers with a pneumatic calibration valve, RAM, 16 bit A/D converter, and a microprocessor in a compact self contained module. The pressure sensors are grouped according to their full scale specification, namely 34.5 barg ($P_{SV}001$–003), 17.2 barg ($P_{SV}004$–09), and 6.8 barg ($P_{SV}010$–016). Given an accuracy of $\pm 0.05\%$ of the full scale of the sensors, the expanded uncertainty for each sensor group is $\pm 0.0.0172$ bar, ± 0.0086 bar, and ± 0.0035 bar respectively. Figure 1b shows eighteen taps situated along the upper and lower nozzle profiles. Two extra taps are located on the flanges of the settling chamber. On the nozzle profile the taps were obtained by boring 0.2 mm diameter holes perpendicular to the profile surface, and afterwards, by drilling a 2.5 mm hole from the opposite side, see detail A. Eighteen 1/16 in. Swagelok tubes are braze-welded to the externally mounted surface of the nozzle profile and separately routed, together with the two tubes connected to the taps of the settling chamber, underneath the nozzle test section to small chambers equipped with sight glasses, i.e., the liquid traps (see ⑪ for the assembly and ⑫ for the valve control panel). This allows to visualise vapor condensation during pressure measurements. To avoid the accumulation of condensate in the lines connecting the pressure taps to the Scanivalve, the pressure scanner is equipped with a nitrogen purging system. The total temperature is measured at the nozzle inlet, see ⑤, with a *Wika TR10-C* PT100 transmitter. The expanded uncertainty is of Class A, i.e., $\pm 0.15 + 0.002\,|T|$ °C as per the EN 60751 standard. The same type of transmitter is also used to measure the temperature, see ⑩, in the receiver.

The adopted schlieren layout is a two-lens flat mirror z-type configuration. The exact same equipment, i.e. light source, pinhole, lenses and camera, employed in the experiment reported in [1] is adopted to visualize gradients of density. In the experiment described in this paper, an additional camera (*BOBCAT IGV-B1610* 16bit CCD) is used to image the nozzle profile geometry, allowing to track changes owing to thermal expansion and, hence, determine the nozzle throat size at various operating conditions.

The operating conditions targeted in the experiment, see Table 1, correspond to the design point of the ORCHID Balance of Plant (BoP) and nozzle test section. Figure 2 displays the thermodynamic states identifying the expansion process in the nozzle under the hypothesis of an isentropic adapted flow. The nozzle TS must be sufficiently prewarmed (at 180 °C for experiments with MM) in order to prevent excessive condensation during the initial stages of the TS operation. Furthermore, due to the inability of gate-valves at the inlet and outlet of the TS to perfectly seal against the flow direction, liquid tends to reside in the receiver during the ORCHID start-up sequence. Thus, when the TS is opened, it is necessary to wait for at least 20 min to allow all the liquid to

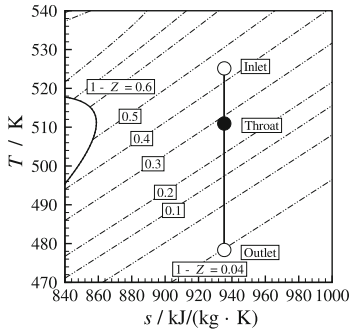

Fig. 2. $T - s$ diagram showing the isentropic expansion for the design conditions of the nozzle (also the target conditions for PR.028-NT.001) with contours of 1-Z (– ···).

Table 1. The target boundary conditions of the experiment PR.028-NT.001.

Fluid	Tot. temp. TT015 / °C	Tot. press. PT011 / bara	Comp. F. Z_{Throat}
MM	252	18.4	0.56
Back p. PT004/bara	Outlet Mach. M_2	Mass flow FT001 /kg/s	
2.1	2	1.145	

evaporate and the operating conditions to stabilize around the values of total inlet pressure and temperature chosen for the experiment. During this settling period, the back pressure PT004 of the nozzle is set to the desired value. Once steady state is achieved, 1,000 schlieren image realisations are acquired at a frequency of 25 Hz, for a total time of 40 s. This ensures the statistical convergence of the measured quantities derived from the schlieren images. Spatial calibration of both cameras is performed by means of a calibration target located at the midspan of the test section, which bears circular markers of 1 mm spacing in both X and Y directions. A pinhole calibration model is employed which additionally accounts for lens distortion. A preliminary observation of the flow patterns in the schlieren images allow to verify if supersonic conditions have been reached in the nozzle and if the fluid is in a dry vapor state, before pressure measurements are carried out. A general outline of the pressure measurement procedure is as follows. The *DSA3218* pressure scanner is pre-warmed one hour before measuring in order to ensure the module becomes thermally stabilized. The pressure lines are purged with nitrogen in order to remove any condensate which may have accumulated during the nozzle starting phase, and which is therefore visible through the sight glass of the liquid trap, see Fig. 1a. Liquid purging ensures that the measuring ports are not blocked by, e.g., dust, metal filaments, tracer particles, and minimises the risk of damaging the transducers while measuring. Additionally, the presence of condensate in the lines is unwanted since it does not allow to correctly measure the flow pressure. The liquid is ejected back into the flow, and this can be checked because the liquid level in the trap must decrease. This procedure normally lasts approximately 10 s. A quick-zero adjustment is then performed and the recording of pressures can begin immediately. In this experiment the pressures are recorded at an acquisition frequency 1 Hz. Simultaneous flow visualization can be performed at this stage of the pressure measurements procedure. Periodic purging and zero-offset corrections must be made, depending on the duration of the pressure recording. For example, if the measurement lasts more than 3 min condensate starts to accumulate in the liquid traps.

3 Data Processing Method and Measurement Uncertainty

The acquired images have been pre-processed using LaVision Davis software version 8.3.0 [7] and subsequently post-processed by means of a Mach line extraction algorithm implemented in a general purpose programming software [13]. In the pre-processing phase, after correcting the dataset for shift and rotation, a spatial calibration has been performed. As a result, the raw distorted schlieren dataset is corrected such that any point in the image sequence corresponds to the correct location in the physical plane.

The Mach line extraction algorithm allows the evaluation of the slope of Mach waves with respect to the local flow velocity (Mach line angle μ) at different axial positions along the nozzle midplane ($Y = 0$) for each frame of the schlieren dataset. The uncertainties associated with both the Mach line angle value and the assigned position in the physical plane are also evaluated, see Ref. [5] for the details. From the Mach line angles, one can estimate the Mach number of the flow on the midplane provided that the flow in the nozzle is symmetric. The flow symmetry is verified by comparing Mach line angles above and below the midplane at different axial coordinates. It was observed that the average values of the angles of two concurring lines do not differ for more than their uncertainty band widths. In addition, the last curved Mach lines of the Kernel region originated both from the top and bottom profile coincide in a point which corresponds to the physical midplane of the nozzle, further proving flow symmetry. As a result, the extracted Mach line angles in the diverging part of the nozzle can be used to calculate, for each image, the corresponding Mach number distribution according to $M = \frac{1}{\sin \mu}$.

The algorithm consists of the following steps. First, the intensity of each image is normalised by dividing the intensity in each pixel by the standard deviation of this quantity calculated over a moving window of 5×5 pixels centered at the pixel being processed. This operation enhances the flow features captured by the schlieren technique. Second, the image is binarized and split in several overlapping interrogation windows, whose size is constant throughout the portion of the image corresponding to the uniform flow region, while it progressively decreases as the Mach lines of interest are closer to the throat. This gradual decrease of the interrogation window size is a function of the local height of the nozzle, and serves to ensure that the curvature of the detected lines does not exceed the local angular resolution. Furthermore, the step between an interrogation window and the next one is chosen to be one third of the width of the previous window. Given the imposed adaptation of the interrogation window size, it follows that the detection algorithm searches for more Mach lines in the kernel region. Third, the Hough transform is applied to each interrogation window [9] and the best line is selected. These operations are repeated for each frame. Finally, once the procedure has been applied to the whole image dataset, it is possible to compute the average and the standard deviation of the angle and length of all the detected Mach lines in each interrogation window. The Mach number distribution along the midplane and its total expanded uncertainty values can then be calculated. For more details on the line extraction algorithm and the uncertainty quantification procedure the reader is referred to [1,5]. Regarding the pressures acquired with the Scanivalve, the statistical averages and standard deviations are directly computed from the measurements obtained in steady conditions.

4 Mach Number Estimation and Static Pressure Measurements

The numerical solutions of the flow-field in the ORCHID nozzle are obtained using the open-source flow solver SU2 for a 2D half-nozzle with symmetry conditions along the midplane. The details about the numerical model, mesh convergence study and the specifications of the used workstation can be found in [3]. However, in this case, variations of specific heat capacity with temperature are considered and the $c_p(T)$ model reported in [10] was used. The critical point properties of MM were taken from [8]. The total inlet conditions assumed in the CFD model correspond to the average total pressure and temperature measured at the nozzle inlet during the experimental run once steady flow conditions established. Their values are $\bar{P}_0$ (PT011) $= 18.36 \pm 0.0229$ bar, $\bar{T}_0$ (TT015) $= 253.7 \pm 0.66$ °C. The pressure measured at the nozzle outlet is $\bar{P}_\mathrm{b}$ (PT004) $= 2.21 \pm 0.0416$ bar.[1] The nozzle profiles considered in the CFD model accounts for the thermal expansion of the nozzle housing. Notably, by analyzing with a dedicated camera the position of markers on the lateral surface of the nozzle profiles, the throat height was determined as $H_\mathrm{th} = 7.73$ mm.

Figure 3a shows the first schlieren image from the recorded sequence, while Fig. 3b represents the same image after the moving filter has been applied to enhance the flow patterns. The average extracted Mach lines are superimposed on the midplane. A shock wave generated by a 5° wedge located at the nozzle outlet has an angle of $\beta_\mathrm{above} = 37.6° \pm 0.86$, and $\beta_\mathrm{below} = 31.6° \pm 0.64$ owing to the axial misalignment of the wedge which occurred during the nozzle TS start up. This will be prevented in the future by means of a more mechanically rigid support system. Figure 3c shows the comparison between the numerical prediction against the Mach number distribution along the nozzle mid-plane obtained experimentally. The experimental data is complemented with the estimated total expanded uncertainty. The axial coordinate x, which represents the distance along the nozzle mid-plane from the throat, is normalized with respect to the nozzle throat height H_th. The extracted Mach number ranges from $M = 1.4 \pm 0.04$ to 1.95 ± 0.05 at positions $x/H_\mathrm{th} = 1.07$ and 7.0, respectively. The Euler simulation predicts higher values for the flow Mach number along the expansion process when compared to the measured Mach number. Nevertheless, the predicted Mach numbers match reasonably well with the experimental results, where the closest match is located inside the kernel region. The deviation tends to increase as the Mach number increases, i.e., towards the nozzle exit. In the uniform region, e.g., after the kernel-uniform transition point, there are two troughs located at $x/H_\mathrm{th} = 4.5$ & $x/H_\mathrm{th} = 6.4$. These troughs are the result of local decreases in the velocity caused by two weak oblique shock waves. This can be explained by the following. The nozzle glass panes have been mounted and sealed with a PTFE gasket giving a flow domain width of 20 mm. There was no loss of pretension on the bolts; the gasket retained its mechanical properties and the thermal expansion coefficient of glass is much lower than that of steel. This indicates

[1] The uncertainty sources associated with the measurements were classified and evaluated as Type A uncertainties (those dependent on measurement statistics) and Type B uncertainties (sensor characteristics) [6]. Type A and B uncertainty values were used to compute the total expanded uncertainty by means of a root sum square. The data acquisition uncertainty was quantified during the calibration of the NI9208 current modules and is deemed negligible.

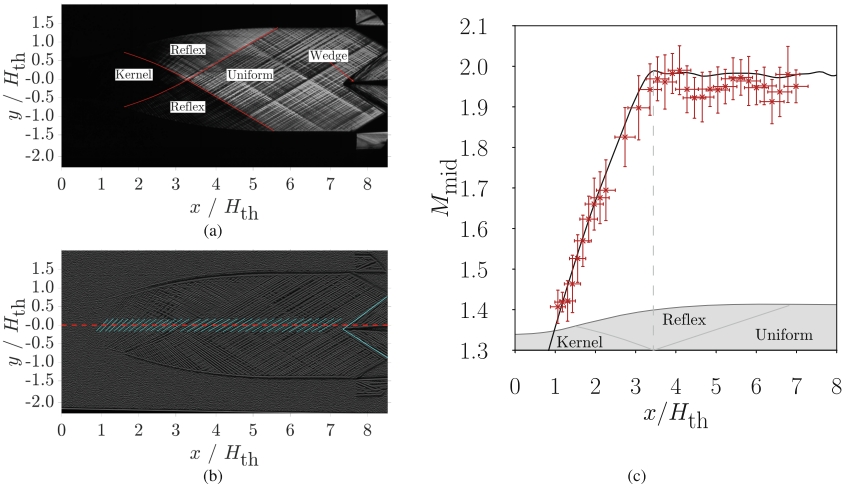

Fig. 3. A non-ideal expansion of MM at the conditions: $\overline{T}_0$ $(TT015) = 253.7$ °C, $\bar{P}_0$ $(PT011) =$ 18.36 bar and $\bar{P}_\mathrm{b}$ $(PT004) = 2.21$ bar. Ref. = throat position. **(a).** A raw schlieren photograph showing Mach waves and an oblique shock wave at the nozzle exit. Knife-edge is horizontal. **(b).** Average extracted Mach lines superimposed on the first post-processed schlieren image. **(c).** Comparison between the measured flow Mach number with the corresponding total exp. uncertainty and the Euler solver numerical prediction.

that the width remained unchanged during the experiments but it will be checked with a confocal displacement sensor (CL-3000 WW) in future experiments. However, the measured nozzle height ratio $H_{\mathrm{Exit,Measured}}/H_{\mathrm{Throat,Measured}} = 2.68 \pm 0.059$ is lower with respect to the design height ratio of $H_{\mathrm{Exit,Design}}/H_{\mathrm{Throat,Design}} = 2.85$. Furthermore, the adapted pressure ratio $P_0/P_{\mathrm{SV}}017 = 8.54$ is also lower than the design pressure ratio of 8.76. This results in a lower nozzle exit static pressure $P_{\mathrm{SV}}017$ than the pressure in the receiver PT004. The mismatch leads to the generation of weak shock waves and the situation of overexpanded flow.

Figure 4 shows the measured static pressure distribution along the top and bottom nozzle profiles complemented with the expanded uncertainty listed in Table 2. Sixteen pressure values located at the indicated tap locations $T\#$ are compared against the results of the Euler simulation together with the computed compressibility factor plotted on the Y2 axis. The match is satisfactory with the greatest deviation inside the kernel and reflex regions; namely, at the Taps T06 = 1.2 %, T08 = 1.4 %, T09 = 2.7 %, T10 = 2.2 %, T13 = 1.7 % and T14 = 1.9%. A small discrepancy is observed at the tap location T17(s) and is most likely due to a small leakage of MM in the line connecting the Scanivalve to the liquid trap.

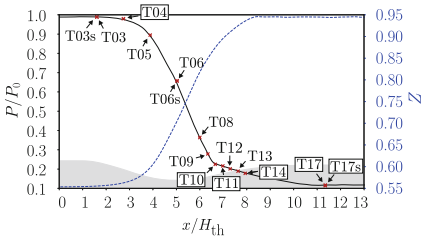

Fig. 4. Static pressures measured along the nozzle during the PR.028-NT.001 experimental run together with the related total expanded uncertainty bars, see Table 2. The pressure is non dimensionalized with the average value of the total pressure at the inlet $\bar{P}_0 = 18.36$ bara and the axial coordinate with the throat height $H_{\text{th}} = 7.73$ mm. Static pressures resulting from the Euler simulation (–) and exp. results (x). The centerline compressibility factor (- -) is calculated with the PR eqn. of state.

Table 2. Scanivalve experimental mean values and related uncertainties for the PR.028-NT.001 test. N.b. taps T01, T07, T15 and T16 not active during this experiment. The total expanded uncertainty includes Type A/B.

Tag	$\bar{P}$ / bara	U / bara *	Tag	$\bar{P}$	U / bara *
T02$^+$	18.33	0.0180	T09	5.11	0.0117
T03	18.15	0.0180	T10	4.12	0.0089
T03s	18.16	0.0180	T11	3.97	0.0037
T04	17.99	0.0179	T12	3.69	0.0037*
T05	16.43	0.0108	T13	3.47	0.0038
T06	12.07	0.0101	T14	3.26	0.0036
T06s	12.06	0.0110	T17	2.15	0.0037
T08	6.68	0.0111	T17s	2.08	0.0035

* Coverage factor $k = 2$. $^+$ T02 in same flange as PT011.

5 Conclusions and Future Work

The SU2 solver is able to accurately predict the flow Mach number and static pressure distribution in a supersonic vapor expansion of the fluid MM. The consistency of the experimental and numerical results indicate that the custom-designed Scanivalve purging and acquisition procedure is effective at measuring static pressures in hot organic vapor flows. Thermal expansion effects are significant and increase the throat height by approx. 3–4%. This decreases the nozzle height ratios ($H_{\text{exit}}/H_{\text{throat}}$) to such a degree that it is apparent in the Mach number results. Tracking the nozzle geometry is thus essential in these experiments. Initial shock wave experiments are promising but the mechanical rigidity of the model support system must be improved. Aligning the model along the axial plane is crucial for models of this size.

References

1. Beltrame, F., Head, A.J., De Servi, C., Pini, M., Schrijer, F., Colonna, P.: First experiments and commissioning of the ORCHID nozzle test section. In: Proceedings of the 3rd International Seminar on Non-Ideal Compressible Fluid Dynamics for Propulsion and Power, NICFD 2020. ERCOFTAC Series, vol. 28, pp. 169–178. Springer, Cham (2021). https://doi.org/10.1007/978-3-030-69306-0_18
2. Conti, C.C., Fusetti, A., Spinelli, A., Guardone, A.: Shock loss measurements in non-ideal supersonic flows of organic vapors. Experiments in Fluids **63**(117), 1114–1432 (2022)
3. Monjas, F., Blanca, H., Adam, J., De Servi, C., Pini, M.: Validation of the SU2 fluid dynamic solver for isentropic non-ideal compressible flows. In: Proceedings of the 4th International Seminar on Non-Ideal Compressible Fluid Dynamics for Propulsion and Power, NICFD 2022. ERCOFTAC Series, ERCO, vol. 28, p. IX, 180. Springer, Cham (2023)

4. Guardone, A., Spinelli, A., Dossena, V.: Influence of molecular complexity on nozzle design for an organic vapor wind tunnel. J. Eng. Gas Turb. Power **135**(4), 042307 (2013)
5. Head, A.J.: Novel experiments for the investigation of non-ideal compressible fluid dynamics: The ORCHID and first results of optical measurements. PhD thesis, Delft University of Technology (2021)
6. International Organization for Standardization (ISO) 1993 Guide to the expression of uncertainty in measurement. Guide 100:2008. Joint Committee for Guides in Metrology, JCGM. Corrected and reprinted (1995)
7. LaVision Inc. Davis, version 8.3.0 (2015)
8. Lemmon, E.W., Bell, I.H., Huber, M.L., McLinden, M.O.: 2018 NIST standard reference database 23: Reference fluid thermodynamic and transport properties-REFPROP, version 10.0, National Institute of Standards and Technology (2018)
9. Lo, R., Tsai, W.: Gray-scale hough transform for thick line detection in gray-scale images. Pattern Recognit. **28**(5), 647–661 (1995)
10. Nannan, N., Colonna, P., Guardone, A., Lemmon, E.: Multiparameter equations of state for selected siloxanes. Fluid Phase Equilibria **244**, 193–211 (2006)
11. Roache, P.J.: Verification and validation in computational science and engineering. Hermosa Publishers, Albuquerque (1998)
12. Robertson, M., Newton, P., Chen, T., Costall, A., Martinez-Botas, R.: 2020 Experimental and numerical study of supersonic non-ideal flows for organic Rankine cycle applications. J. Eng. Gas Turbines Power **142**(8), 081007 (2020)
13. The MathWorks, Inc. 2019 MATLAB version 9.7.0.1261785 (R2019b) Update 3
14. Zocca, M., Guardone, A., Cammi, G., Cozzi, F., Spinelli, A.: Experimental observation of oblique shock waves in steady non-ideal flows. Exp Fluids **60**(6), 101 (2019)